Influence of the Crystalline Structure in the Segmental Mobility of Semicrystalline Polymers: Poly(ethylene naphthalene-2,6-dicarboxylate)

A. Nogales,† Z. Denchev,‡ I. Šics,§ and T. A. Ezquerra*

Instituto de Estructura de la Materia, C.S.I.C., Serrano 121, 28006 Madrid, Spain

Received June 20, 2000

ABSTRACT: The influence of the characteristic nanostructure of semicrystalline polymers on the segmental dynamics has been studied by dielectric spectroscopy (DS) in poly(ethylene naphthalene-2,6 dicarboxylate) (PEN) samples with different degree of crystallinity. In the investigated temperature range (from −100 to +200 °C), three processes have been identified as maxima in the imaginary part of the complex dielectric permittivity (ϵ^*). The shape of the α-relaxation has been analyzed on the basis of the Havriliak−Negami formalism. Two different levels of restrictions have been found for low and high crystallinity samples. Results from DS and from differential scanning calorimetry (DSC) indicate that the amount of material involved in the α process is smaller than the one calculated on the basis of crystallinity. Both effects further support the existence in semicrystalline polymers of an heterogeneous amorphous phase with regions of different levels of mobility.

1. Introduction

The molecular motions occurring in the amorphous phase of a semicrystalline polymer present characteristic aspects which depend, in a first approximation, on the degree of crystallinity.[1] In semicrystalline polymers at temperatures higher than the glass transition temperature, T_g, the amorphous polymer chains are confined to move between the crystalline regions.[1−3] This restriction modifies the dielectric α relaxation which is detected in polymeric systems at temperatures above T_g. It is known that this relaxation involves motions extended to several molecular segments. The existence of crystallinity in a polymer is reflected in the dynamics of the α-relaxation, when compared with that of the pure amorphous polymer, by three effects: (a) a decrease of the intensity of the relaxation, (b) an increase of the relaxation time and (c) a concurrent change in its shape.[1,2,4,5] However, when dealing with the dynamics of the amorphous phase in a semicrystalline polymer, the crystallinity itself is not enough to characterize the system, and profound information about the microstructure, i.e., the way this crystallinity is distributed along the sample, is needed.[6] Recent experiment have shown that, in general, the microstructures of semicrystalline polymers consist of a complex puzzle of crystalline lamellae, crystal−amorphous interphases,[7] stacks of crystalline lamellae,[8] liquid pockets,[9] rigid amorphous phases,[7] and fringed micellar crystals.[10] The arrangement of this structural elements in a given polymer depends on different factors, including chemical structure, chain flexibility, thermal history, and orientation.[11−14]

Poly(ethylene naphthalene-2,6 dicarboxylate) (PEN) is a semiflexible polyester which has found different applications for engineering purposes.[15] PEN is a polymer stiffer than poly(ethylene terephthalate) (PET) because it contains a naphthalene ring instead of the benzene ring of PET. This fact provides a higher glass transition temperature to PEN (T_g = 117 °C), when compared to PET (T_g = 75 °C), and a slower crystallization kinetics.[16] It has been reported that PEN is able to crystallize in two possible modifications. The more common one, called α-modification, is a triclinic crystal lattice which is obtained by usual thermal treatment of the amorphous phase. The less usual β-modification is also triclinic, and can be obtained by means of a special spinning or annealing processes.[17] Previous investigations of the dynamical properties on a narrow frequency range of amorphous PEN by dynamical mechanical analysis (DMA),[18] nuclear magnetic resonance (NMR),[19] and dielectric spectroscopy (DS)[20,21] have shown the existence of three relaxation processes. Arranged in order of increasing temperature, these relaxations correspond to the local motion of ester groups (β), a local motion of the naphthalene ring (β^*), and the α-relaxation at $T > T_g$.

The aim of the present work is to determine the effect of the nanostructure developed upon crystallization on the segmental relaxation appearing in PEN by selecting specific samples in which a thorough characterization of the structure has been accomplished.

2. Experimental Part

Pelleted PEN (Eastman, average viscosity molecular weight $M_v \approx 25\,000$) was melted and pressed at a temperature of 290 °C for 2 min, under slight pressure. The original pellets were previously dried enough to ensure that during the melting and pressing hydrolyzation does not take place. In this way, amorphous films of 0.2 mm thickness were produced. Samples with specific crystallinity were obtained by introducing the films into a tightly closing stainless steel chamber placed into a vacuum oven at a selected temperature (T_a) for a given annealing time (t_a).[22] The thermal history of the investigated samples is reported in Table 1.

The mass crystallinity fraction (X_c^{WAXS}) was determined by means of WAXS a peak deconvolution method.[6] Volume crystallinity (X_c^{ρ}) was obtained by density measurements through

$$X_c^{\rho} = \frac{\rho - \rho_a}{\rho_c - \rho_a} \quad (1)$$

† Present address: J.J. Thomson Physics Laboratory, University of Reading, Witheknights, Reading RG6 6AF, U.K.

‡ Permanent address: University of Minho, Campus Azurém, Guimaraes, Portugal.

§ Permanent address: Riga Technical University, Institute of Polymers Materials, 14 Azenes St. Riga LV 1048, Latvia.

10.1021/ma001066h CCC: $19.00
Published on Web 11/18/2000

where $\rho_a = 1.3301$ g/cm^3 and $\rho_c = 1.4007$ g/cm^3 are the densities of amorphous and crystalline phases respectively.[22]

The density of the samples was measured in a gradient density column using a mixture of *n*-hexane and tetrachloromethane. The range was selected to allow measurements in the range between 1.3200 and 1.4100 g/cm^3. For the dielectric experiments, circular gold electrodes, 3 cm in diameter, were deposited onto the film surfaces by sputtering. Measurements of the complex dielectric permittivity, $\epsilon^* = \epsilon' - i\epsilon''$, were performed over a frequency window of 10^{-1} Hz $< F < 10^5$ Hz in a temperature range of -100 °C $< T < +200$ °C. To cover the above frequency range, a Novocontrol system integrating a SR 830 lock-in amplifier with a dielectric interface was employed. The temperature in these experiments was controlled by a nitrogen jet with a temperature error, during every single sweep in frequency, of ±0.1 °C.

The dielectric relaxations were phenomenologically described in terms of the Havriliak−Negami (HN) equation

$$\epsilon^* = \epsilon_\infty + \frac{\epsilon_0 - \epsilon_\infty}{[1 + (i\omega\tau)^b]^c} \tag{2}$$

where ϵ_0 and ϵ_∞ are the relaxed ($\omega = 0$) and unrelaxed ($\omega = \infty$) dielectric constant values, τ is the central relaxation time of the relaxation time distribution function, and b and c ($0 < b$, $c < 1$) are shape parameters which describe the symmetric and the asymmetric broadening of the relaxation time distribution function, respectively.[23] According to the HN approach, eq 2 can be used to derive the corresponding analytical expressions of the imaginary part of the dielectric permittivity

$$\epsilon'' = (\epsilon_0 - \epsilon_\infty) r^{-c} \sin(c\psi) \tag{3}$$

with

$$r^2 = 1 + 2(\omega\tau_0)^b \cos(b\pi/2) + (\omega\tau_0)^{2b} \tag{4}$$

and

$$\tan\psi = \frac{(\omega\tau_0)^b \sin(b\pi/2)}{1 + (\omega\tau_0)^b \cos(b\pi/2)} \tag{5}$$

To analyze the shape and temperature evolution of the α relaxation at low frequencies a conduction term was added to ϵ'':

$$\epsilon''_{cond} = \frac{\sigma}{\epsilon_{vac}\omega^s} \tag{6}$$

where σ is related to the direct current electrical conductivity, ϵ_{vac} is the vacuum dielectric constant, and s is related to the nature of the conduction mechanism. A value of $s < 1$ is related to a nonohmic transport.[24] A subroutine based on the Newton method[5] was modified to fulfill our requirements and was used in the fitting. To estimate the accuracy of the fitting parameters, their values have been varied. We found that the maximum possible variation without provoking a significant deviation between the measured and calculated curves was less than ±5% for b, c, and $\Delta\epsilon$, and ±10% for τ_0.

X-ray experiments were performed by means of a Seifert XRD 3000 θ/θ diffractometer using Ni-filtered Cu Kα, radiation at a scanning speed of 0.02°/s. Small-angle X-ray scattering (SAXS) experiments were performed at HASYLAB (Hamburg, Germany). SAXS data analysis was accomplished as described elsewhere.[22] The thermal behavior of the samples was analyzed by using a Perkin-Elmer 7 differential scanning calorimeter at a heating rate of 10 °C/min under a nitrogen atmosphere. The temperature and heat flow scale of the calorimeter were calibrated with indium.

3. Results

3.1. Sample characterization. The WAXS diffraction patterns of the investigated samples with increasing crystallinity from 0 to 0.27 are presented in Figure 1. The Bragg peaks appearing in the diffractograms of all the sample correspond to the [010], [100], and [$\bar{1}$10] reflections of the α modification of PEN. Values for X_c^{WAXS} are reported in Table 1. Figure 2 shows the DSC traces of the investigated samples. A magnification of these traces at the glass transition region of the studied PEN samples are presented as an inset in Figure 2. From the heating scan, the glass transition temperature was determined to be the temperature of half step in the heat flow. This jump can be obtained from the intersection of both, the extrapolation of the glassy line and that the liquid line with the line of maximum heat flow variation. The corresponding values of ΔC_p and the melting enthalpy are shown in Table 1. Previous investigations have shown that semicrystalline PEN samples consist on a heterogeneous distribution of crystalline lamella stacks.[22] The long period, L, the thickness of the crystalline lamella, l_c, and that of the amorphous layer, l_a (Table 1), of the stacks were determined from the one-dimensional electron density correlation function obtained from the small-angle X-ray scattering patterns.[9,22] Long period values ($L \approx 110$ Å) were detected only for samples with X_c^{WAXS} higher than 0.13.

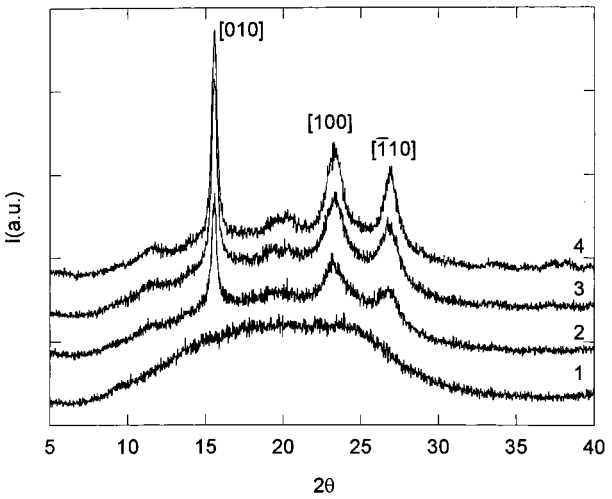

Figure 1. WAXS diffractograms of the PEN samples with different degrees of crystallinity.

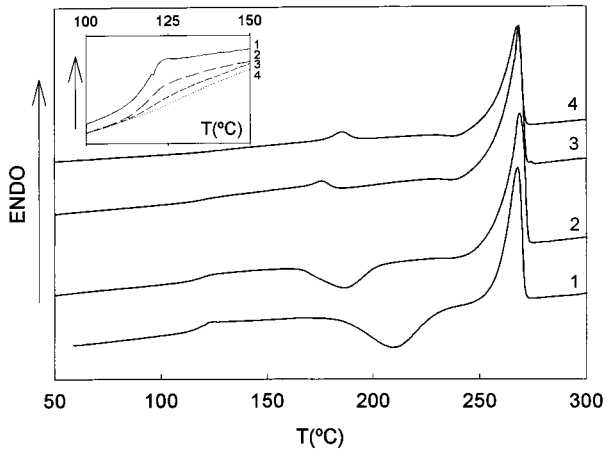

Figure 2. DSC traces of the PEN samples with different crystallinity. The inset shows an example a magnification in the region of the glass transition temperature.

3.2. Dependence of the Dielectric Relaxation with Crystallinity. Dielectric loss (ϵ'') values measured

Table 1. Description of the Investigated Samples

sample	T_a	t_a	χ_c^{WAXS}	χ_c^{ρ}	ΔH_m (J·g^{-1})	ΔC_p (J·g^{-1}·K^{-1})	L (Å)	l_c (Å)	l_a (Å)
1			0.00	0.00		0.33			
2	145	200	0.13	0.08	28.4	0.28			
3	165	200	0.20	0.27	50.7	0.12	110	75	35
4	165	1440	0.27	0.33	52.0	0.07	110	76	34

[a] Key: annealing temperature, T_a; annealing time, t_a; mass crystallinity of the samples determined by WAXS, χ_c^{WAXS}; volume crystallinity, χ_c^{ρ}; enthalpy of melting, ΔH_m; height of the jump at the glass transition, ΔC_p; long spacing determined by SAXS, L; thicknesses of the crystalline and amorphous layers, l_c and l_a.

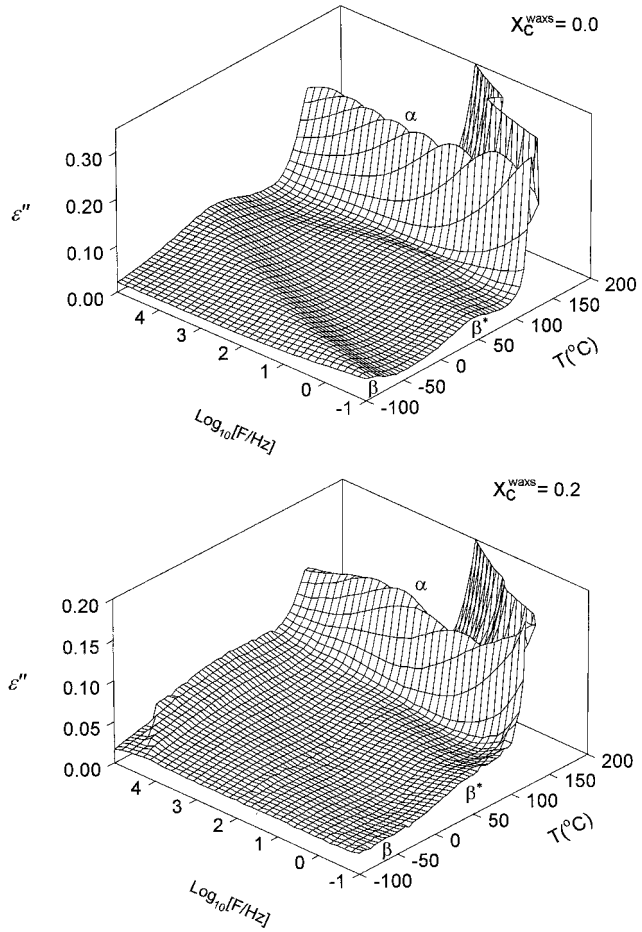

Figure 3. ϵ'' values for two selected PEN samples with different crystallinity as a function of frequency and temperature.

as a function of temperature and frequency for two samples with $\chi_c^{WAXS} = 0$ and $\chi_c^{WAXS} = 0.2$ are illustrated in Figure 3. As expected three main dielectric relaxations, β, β*, and α, appear in the order of increasing temperature according to the literature.[18,20] The relaxation processes appear as maxima in ϵ'' moving toward higher temperatures when the frequency is increased. The α process is the most prominent one while both the β and the β* are much less intense. For the semicrystalline samples, the intensity of the three dielectric relaxations is strongly reduced when comparing with the spectrum of the amorphous sample. The position in temperature of both, β and β* relaxations remains almost unaffected when crystallinity increases. On the contrary, the α-relaxation shifts toward higher temperatures and its intensity decreases when crystallinity increases. This indicates that the α-relaxation is more

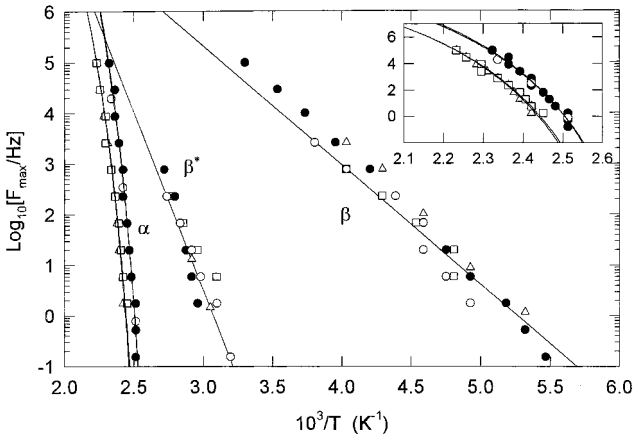

Figure 4. Dependence of the frequency of maximum loss (F_{max}) with the reciprocal temperature for the relaxations in PEN samples with different degrees of crystallinity: (○) $X_c^{WAXS} = 0.00$, (●) $X_c^{WAXS} = 0.13$, (□) $X_c^{WAXS} = 0.2$, and (△) $X_c^{WAXS} = 0.27$. Continuous lines represent Arrhenius fits for β- and β*-relaxations and Vogel−Fulcher−Tamann fits for the α-relaxation.

Table 2. Vogel−Fulcher−Tamann Parameters for PEN Samples with Different Crystallinity

sample	F_0 (Hz)	A (K)	T_0 (K)	D
1	9.8×10^{13}	1898.6	340.2	5.6
2	9.8×10^{13}	1839.5	342.2	5.4
3	1.0×10^{13}	1844.2	347.6	5.3
4	1.0×10^{13}	1828.4	349.1	5.2

sensitive to changes in the microstructure than the β and the β* ones. The changes in shape will be analyzed latter in more detail according to the HN formalism.

The frequency of maximum loss, F_{max}, have been represented in Figure 4 as a function of the reciprocal temperature for all the studied samples. The HN formalism described in the next paragraph was used to determine F_{max} values for every relaxation. In such a representation, the β and β* relaxations follow an Arrhenius behavior revealing them as local noncooperative thermally activated processes. In the case of both β and β* relaxations, F_{max} values for samples with different crystallinity lie in a similar range. From the slope of the straight line obtained it is possible to get the activation energy of both processes. In the case of β relaxation a value of $\Delta E = 13$ kcal/mol is obtained. For the β* relaxation, the activation energy is larger, around $\Delta E = 33$ kcal/mol. In the case of the α-relaxation, the dependence of $\log_{10}[F_{max}]$ with the reciprocal temperature shows a certain curvature (see inset in Figure 4 for magnification) which can be described by means of the Vogel−Fulcher−Tamann (VFT) equation:

$$F_{max} = F_0 \exp[-A/(T - T_0)] \qquad (7)$$

The VFT parameters, F_0, A, and T_0 are presented in Table 2. The obtained values for the Vogel temperature T_0 increases with crystallinity and the preexponential factor F_0 shows different values for the samples with $\chi_c^{WAXS} < 0.2$ than for the samples with higher amount of crystallinity.

3.3. Phenomenological Analysis of the Dielectric Data of the α-relaxation. Figure 5 shows ϵ'' values as a function of frequency for three selected samples in the temperature region of the α-relaxation. It is observed that crystallinity induces a strong influence on the shape of the α relaxation. For the amorphous and

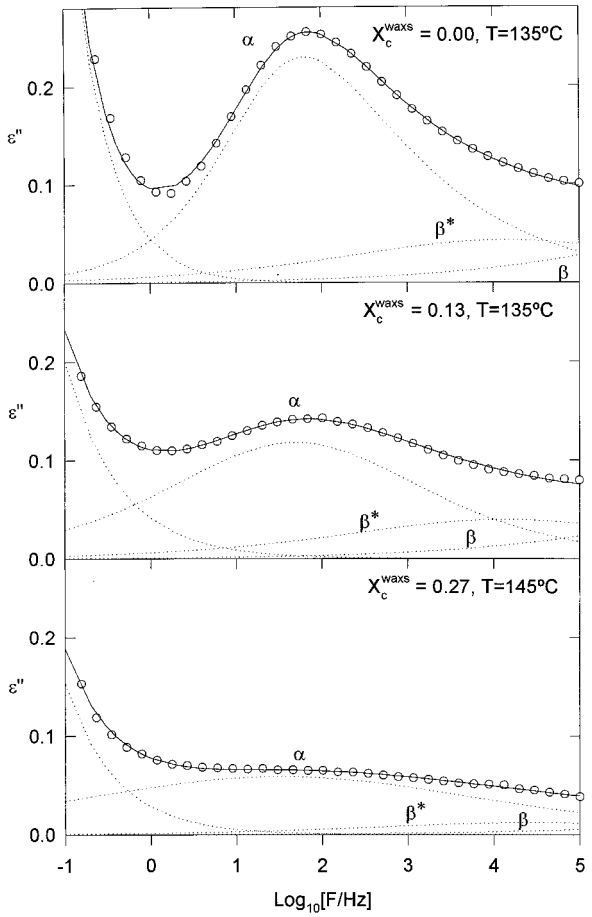

Figure 5. ϵ'' values for three selected PEN samples: 1, 2, and 4 as a function of frequency (F) for different temperatures. Continuous lines represent best fits according to Havriliak−Negami equation. Dashed lines shows the separated contribution of the relaxation and the conduction process.

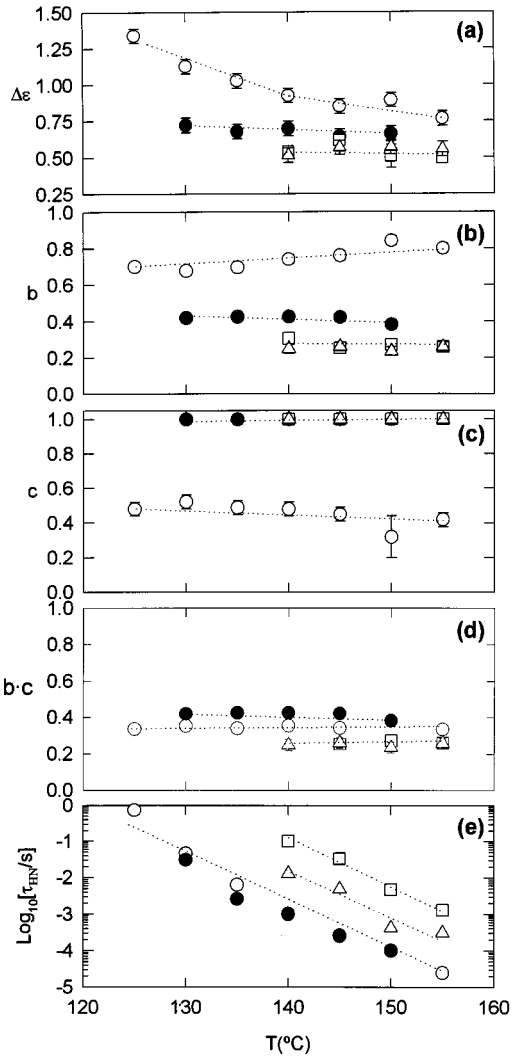

Figure 6. $\Delta\epsilon$, b, c, bc, and τ(HN) parameters for PEN samples with different crystallinities. Symbols as in Figure 4. Continuous lines are eye guides.

for the sample with $\chi_c^{WAXS} = 0.13$, $F_{max} \approx 10^2$ Hz for $T = 135$ °C while for samples with higher crystallinity the α-relaxation shifts to higher temperatures as compared with the α-relaxation of the amorphous sample. To attempt a description of the relaxations by the HN formalism one must consider that at high frequencies the tails of the low-temperature relaxations (β and β*) influence the α-relaxation. Because of the fact that the experimental frequency range does not cover, in the temperature range where the α maximum appears, the β and β* process, these must be simulated in order to correctly fit ϵ''. An extrapolation procedure similar to that used by Coburn and Boyd[1] was used, modified in the case of PEN to consider (i) the influence of the β relaxation in the region where β* appears and (ii) the influence of these two relaxations in the α relaxation. Further details have been reported in the Appendix. The solid lines in Figure 5 represent the best fits according to the Havriliak−Negami equation. Dashed lines represent separated contribution of the different relaxation processes and the conduction process. The parameters obtained in the case of the α-relaxation for the amorphous and the semicrystalline samples are presented in Figure 6 as a function of temperature. $\Delta\epsilon$ values for the α-relaxation of the amorphous sample, presented in Figure 6, decrease strongly with temperature. The semicrystalline samples show smaller values of $\Delta\epsilon$ with a different temperature dependence. In the semicrystalline samples, $\Delta\epsilon$ either remains constant with temperature, or exhibits a slight increase. In the studied temperature range, the α relaxation of the amorphous sample becomes narrower as temperature increases as evidenced by the increase of the b parameter. The presence of some crystallinity, even if it is in small amounts, changes dramatically the shape of the α-relaxation. The α-relaxation becomes broader as revealed by the fact that the b parameters are considerably smaller than those of the amorphous sample and they exhibit almost no temperature dependence. The crystallinity also affects the asymmetry of the relaxation. The amorphous sample presents an α-relaxation which is strongly asymmetric, with an asymmetric broadening parameter $c \approx 0.4$ nearly constant in the studied temperature range. This feature is changed by the presence of the crystalline regions. Even for the samples with lower amounts of crystallinity, the relaxation becomes symmetric, as revealed by the maximum possible value of c ($c = 1$).

4. Discussion

4.1. The β and β*-Relaxations. The β-relaxation of PEN appears at similar temperatures as in the case of PET[1] and even more flexible polyesters.[6] The activation energy of this β-process is around 13 kcal/mol, which

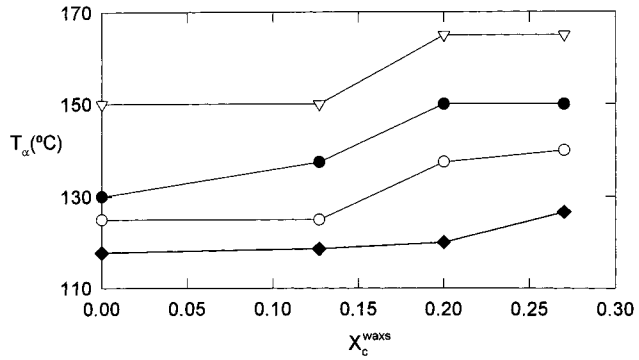

Figure 7. α-Relaxation temperature for PEN (T_α) as a function of crystallinity. Different symbols represent different frequencies: (○) 10^0, (●) 10^2, and (▽) 10^4 Hz. The values of the calorimetric glass transition are also included (◆).

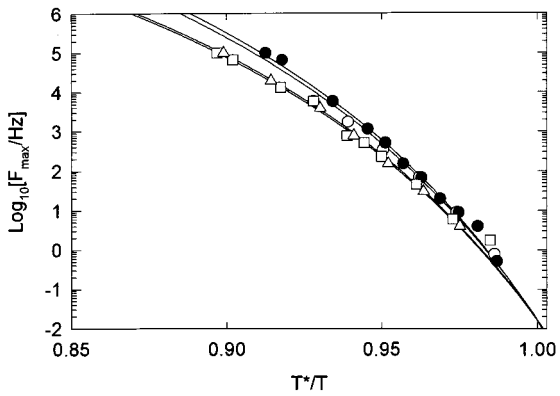

Figure 8. Cooperativity plot: F_{max} vs T^*/T for PEN with different crystallinity. T^* is the calculated temperature at which $\tau = 1/(2\pi F_{max}) = 10$ s. Symbols are as in Figure 4. Continuous lines represent the best fit to the data according to the VFT equation.

corresponds to the local motion of the ester groups.[1] While the PEN chemical structure is similar to that of PET, the relaxation spectra of both polymers are drastically different, because of the presence of the β^*-relaxation in PEN. One must consider that the repeat unit of PEN differs from that of PET by the presence of a naphthalene group instead of a benzene group. The naphthalene group is not symmetric related to the main chain axis. Then, the motions of this group around the main chain imply changes in the dipolar motion, and could be detectable by dielectric spectroscopy measurements originating the β^* process. In the case of PET, for symmetry reasons, the flips of the benzene group around the main chain do not imply changes in the dipolar moment, and it cannot be detectable by dielectric spectroscopy measurements. However, this motion of the benzene ring can be observable by other techniques like nuclear magnetic resonance (NMR). Such "phenyl flip" motions exhibit an activation energy on the order of ≈8 kcal/mol.[25] The activation energy of the β^*-relaxation is relatively high (≈33 kcal/mol) for local relaxations. This fact can be understood taking into account the high volume of the naphthalene group as compared to that of the phenyl group. Because of the local nature of both the β and β^*, the existence of crystallinity only affects, in a first approach, the intensity of the process.

4.2. Influence of the Crystallinity on the Mobility of the Amorphous Regions above T_g. 4.2.1 Temperature Range of the α-Relaxation as a Function of Crystallinity. Figure 3 shows that the temperature position of the sub-glass relaxations is not affected by the presence of the crystalline regions. However in Figure 3 is clearly seen that crystallinity produces on the α-relaxation a shift toward higher temperatures. A similar feature is observed for T_g as measured by DSC. This effect is also reflected in the isothermal plots (Figure 5). The α-relaxation appears to be shifted toward higher temperatures, for the samples with crystallinity higher than 13%. Figure 7 represents the temperature of maximum loss for the α-relaxation (T_α) at different frequencies for the investigated samples as a function of crystallinity. It is observed that the difference between T_α for the amorphous sample and for the sample with $X_c^{WAXS} = 0.13$ is almost negligible. However, a clear increase of T_α is observed for samples with higher amounts of crystallinity. For comparison, the values of the calorimetric T_g are also included in Figure 7. As one sees, T_g and T_α follow a similar tendency although the upward shift of T_g occurs for higher values of crystallinity. For the higher values of crystallinity, this behavior is slightly different to the observed in PET where a progressive increase of T_α with χ_c is found.[1,26] In PEN, it is observed that, for $\chi_c^{WAXS} > 0.2$, F_{max} values seem to be independent of crystallinity (see inset in Figure 4).

The strong fragile scheme proposed by Angell allows one to classify glass forming liquids on the basis of the temperature dependence exhibited by the relaxation time (τ).[27,28] By scaling τ values as a function of T^*/T, where T^* is a reference temperature, the relaxation time temperature dependence of systems with different T_g can be compared. Within this scheme, the fragility of a system is defined as the degree of departure from the Arrhenius behavior exhibited by the relaxation time of the a relaxation process. In polymers, fragility has been associated with the strength of the correlation between non bonded species and has been renamed cooperativity.[28] Relaxation experiments comparing polymers in both the amorphous state and the semicrystalline state have shown that, despite the observed shift in T_g, a rather similar dependence of the relaxation time with T^*/T (cooperativity plot) is observed.[29,30] Our dielectric experiments performed in PEN samples with varying crystallinity reveal a temperature dependence of F_{max} corresponding to the α-relaxation strongly deviating from an Arrhenius behavior (Figure 4). To quantify this deviation, the parameter A from the VFT equation (eq 7) can be replaced by DT_0 where D is called the fragility strength.[28] In Figure 8, we have replotted the F_{max} data of Figure 4 as a cooperativity plot (F_{max} vs T^*/T) where T^* is a reference temperature calculated from the VFT equation, as the absolute temperature at which $\tau = 10$ s ($\tau = 1/(2\pi F_{max})$). Although the PEN samples with different crystallinity exhibit different T^* values, upon scaling by T^*/T, low F_{max} values tend to collapse at low frequencies into a single curve as predicted by Ngai et al.[29] However, at higher frequencies, there are two clear tendencies. On one hand the amorphous sample, and the sample with 13% of crystallinity tend to a high value of frequency (F_0) at high temperatures. On the other hand, samples with crystallinity amounts higher than 13% tend to a slightly smaller F_0 value.

As shown in Figure 5,, the presence of crystallinity results in a broadening of the α-relaxation as characterized by a decrease of the b parameter. In amorphous polymers the α-relaxation is generally asymmetric. This is the case for amorphous PEN, as revealed by the

asymmetry parameter $c < 1$ (Figure 6). The presence of crystals produces a broadening and a symmetrization of the relaxation. In our case, the investigated semicrystalline samples seem to follow the above mentioned features (see Figure 6). The α-relaxation of the semicrystalline samples is symmetric, even in the samples with very small amount of crystallinity. The broadening parameter b, however, changes gradually with increasing the crystallinity. Schlösser and Schönhals have shown that the shape parameters can be related to the molecular dynamics at the glass transition provided that the molecular mobility is controlled by inter- and intramolecular interactions.[31] This phenomenological model relates the *b* parameter to the large scale motions and the *bc* product to the small scale motions. Experimental support of the model has been provided by DS techniques.[32] In addition, this model allows one to interpret the observed broadening and symmetrization of the α-relaxation in polymers during crystallization as due to the restriction in the large scale motions of the polymeric chains as the material is filled in with crystals.[5,6] As the crystallinity increases, restrictions to the possible available conformations appear.[1] Segments of the polymer chains included in the crystals hinder the overall mobility of the bonded segments in the amorphous phase. According to this model,[31] this hindered mobility affects more the large scale motions rather than the small scale ones. Our results show that a small amount of crystallinity ($\chi_c^{WAXS} = 0.13$) is enough to restrict the large scale motions occurring on the amorphous phase, as revealed by the dramatic decrease of the *b* parameter. However, the situation is different as far as the short scale motions are concerned. Figure 6 shows the product *bc* for the samples studied here, as a function of temperature. In this figure is clearly seen that *bc* values are only slightly dependent on crystallinity. One explanation of this fact is that a very small amount of crystallinity is enough to perturb the large scale modes in the motion of the amorphous chains. However, the short scale modes of the amorphous segments in the low crystallinity sample present dynamic characteristics similar to those of the chains in a fully amorphous sample. This is in accordance with the fact that, the position of the α-relaxation (T_α) is similar to that of the amorphous sample. Samples with higher amount of crystallinity display higher values of T_α.

4.2.2. Mobile Fractions above T_g. It is evident that the presence of crystallinity reduces the amount of relaxing material because the material incorporated within the crystals does not contribute to the α-relaxation process. However, there is experimental evidence that the crystalline phase is not the only fraction of material which remains rigid at temperatures above T_g.[30,33,34] On the contrary, it was shown the existence of another portion of the amorphous phase, with no three-dimensional order but with restricted mobility above T_g. This phase has been referred to as the rigid amorphous phase (RAP) and indicates the heterogeneity of the dynamic characteristics of the amorphous fraction in semicrystalline polymers. One possibility to estimate the amount of the mobile fraction, χ_{mf}, is by using the ratio between the relaxation intensity of the semicrystalline sample and that of the amorphous sample. From the calorimetric experiments, the mobile amorphous fraction can be estimated as[7]

$$\chi_{mf}^{DSC} = \frac{\Delta C_p^{sc}}{\Delta C_p^{a}} \tag{8}$$

In eq 8 ΔC_p^{sc} is the step height of the specific heat capacity of the semicrystalline sample and ΔC_p^{a} is that for the completely amorphous sample. In Figure 9 the mobile fraction obtained by DSC at the glass transition temperature has been presented as a function of the crystallinity. Here, the left part of the horizontal error bars corresponds to χ_c^{WAXS} while the right part corresponds to χ_c^{ρ}. There is a clear decrease of χ_{mf}^{DSC} with both mass and volume crystallinity. For all the samples, χ_{mf}^{DSC} is smaller than expected considering the total amount of noncrystalline material ($1 - \chi_c$). The data seem to follow a linear trend, which extrapolates to $\chi_{mf}^{DSC} = 0$ for a very low value of crystallinity of around 40%. According to that samples with crystallinity higher than this value would exhibit no relaxation at the glass transition region as detected by DSC. In an analogous way, the fraction of mobile amorphous material can be estimated from the ratio between the dielectric relaxation strength of the semicrystalline sample and that of the fully amorphous one. There are two criteria in the literature for the selection of the values of $\Delta\epsilon$ to be normalized. One of them is to consider the values of $\Delta\epsilon$ for the different samples at a given temperature.[33] The second one is to consider $\Delta\epsilon$ for the relaxation processes of the different samples with the same frequency of maximum loss (F_{max}).[26] This second criteria would lead to a less arbitrary election if all the considered relaxation processes were symmetric. Having the same F_{max} would be similar to have similar central relaxation time. However, this is not the case here, since the relaxation process for the completely amorphous sample is asymmetric as revealed by the shape parameter $c < 1$. Relaxations with different asymmetry parameters but the same F_{max} do not have the same central relaxation time;[23] hence, this election of $\Delta\epsilon$ is also arbitrary. For this reason, for the sake of comparison, we have considered $\Delta\epsilon$ measured at the same temperature. Thus, the mobile fraction at a given temperature, determined by DS is given by[33]

$$\chi_{mf}^{DSC} = \frac{\Delta\epsilon_{sc}(T)}{\Delta\epsilon_{a}(T)} \tag{9}$$

In eq 9 $\Delta\epsilon_{sc}(T)$ is the dielectric strength of the a relaxation of the considered sample at a certain temperature T and $\Delta\epsilon_a(T)$ is that for the amorphous sample at the same temperature. In Figure 9 the mobile fraction obtained by DS at $T = 145$ °C has been also presented as a function of the crystallinity. The amount of mobile fraction obtained by DS seems to follow a linear decreasing behavior, which in this case extrapolates to $\chi_{mf}^{DSC} = 0$ for a value of crystallinity of around 72%. The determinations of the mobile amorphous fraction by DSC or by DS, present a crucial difference. According to Figure 9, samples with crystallinity values higher than 40%, would exhibit no relaxation by DSC. However, at higher temperatures, they would show a relaxation process detectable by DS. One explanation for this finding could be that in the temperature interval between T_g and the considered temperature (in this case $T = 145$ °C) some morphological changes occurs, changing then the topology of the restrictions imposed by the

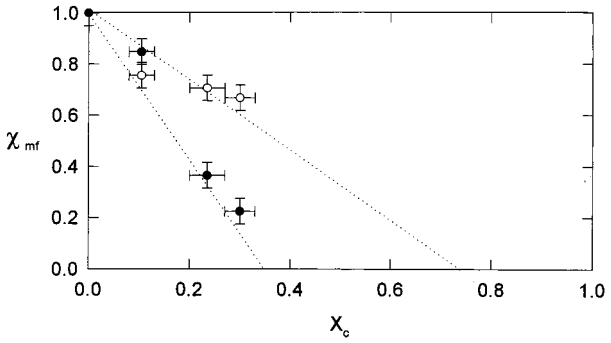

Figure 9. Amorphous mobile fraction of the studied samples determined by DSC, χ_{ma}^{DSC} (●), at the glass transition temperature and determined by DS, χ_{ma}^{DS} at T = 145 °C (○), as a function of crystallinity. The left limit of the horizontal error bar corresponds to X_c^{WAXS} while the right part corresponds to X_c^{ρ}.

crystals to the motion of the amorphous phase. However, this is not the case for PEN, as can be deduced from the DSC scans (Figure 2). A more likely explanation may be given by considering the cooperative character of the α-relaxation. This fact implies that the segmental motions are correlated up to a certain distance ξ_α. According to the Adams and Gibbs theory, ξ_α increases with decreasing temperature,[35,36] and the restrictions imposed by the crystals become more effective when the size of the mobile amorphous regions matches $2\xi_\alpha$.[36] For amorphous PET, ξ_α at T_g has been reported to be ≈1.6 nm.[36] Considering the larger extension of the PEN monomer, a higher value of ξ_α is expected. According to that for PEN at T_g, the α-relaxation is expected to be highly restricted because $2\xi_\alpha$ will be >3.2 nm which is in the range of the calculated amorphous layer on the crystalline stacks (Table 1). Consequently, at the glass transition, the cooperative motions in the constrained amorphous regions are expected to be effectively inhibited. However, when the temperature increases, a decrease of ξ_α occurs activating shorter length scale modes which may be eventually detected by DS. Similar arguments have been recently used to explain the dynamic bevaviour PVDF−PMMA blends[37] and agree with the existence in PEN of a rigid amorphous phase (RAP) which gradually relaxes when the temperature is increased well above T_g.[13,33]

5. Conclusions

Dielectric spectroscopy was used to characterize in a broad frequency range the dynamics of the α-relaxation of PEN with different crystallinity. Three relaxation processes, β, β*, and α are detected in the measured frequency and temperature windows. The β process can be associated with the local motions of the ester groups in the main chain.The β*-relaxation shows an unusual high activation energy, and can be attributed to the local motion of the naphthalene ring, detectable by dielectric spectroscopy due to the asymmetry of this group. The α relaxation is attributed to the segmental motions taking place in the amorphous phase at temperatures above the T_g. The characteristics of the α-relaxation depend on crystallinity in a peculiar way. The short scale modes of the α-relaxation in samples with crystallinity less than 13% are very similar to those of the amorphous material. However, a small amount of crystallinity is enough to affect the long scale modes of the α-relaxation. In samples with higher crystallinity, short and large scale motions are affected by the presence of crystallinity, but small scale motions are less affected. For identical crystallinities, the mobile amorphous fraction calculated on the basis of the strength of the dielectric relaxation at high temperatures is much higher than the one calculated by DSC. Both effects support the existence, in semicrystalline polymers, of an amorphous phase with regions of different degrees of mobility that may be activated as the temperature increases.

Acknowledgment. The authors are indebted to the DGICYT (Grant PB 94-0049), Spain, and to Comunidad deMadrid (07*N*/0063/1998) for the generous support of this investigation. A.N. thanks the Spanish Ministry of Science for the tenure of a fellowship of the FPI program. I.Š. gratefully acknowledges financial support from the Spanish agency for international cooperation, A.E.C.I. Z.D. acknowledges the tenure of fellowships granted by NATO and MEC (Spain) (5B97-K5447945). Continuous encouragement and useful comments from Prof. F. J. Baltá-Calleja are highly appreciated.

Appendix

Extrapolation Procedure. As mentioned in the Results, the Havriliak−Negami parameters were obtained following an extrapolation procedure similar to that proposed by Coburn and Boyd[1] modified for PEN to consider the β* relaxation. In this appendix we have included as an example, the procedure followed for the amorphous sample. Figure 10 shows the experimental data obtained for the β*- and α-relaxation at those temperatures for which the central relaxation time is ≈7 × 10^{-3} s. In the case of the β-relaxation, this corresponds to a temperature of T = −65 °C. The dashed line in the figure corresponds to the best fit of eq 2 to the experimental points. By doing so for all the temperatures where the maximum of loss is well defined within the experimental window, a series of HN parameters is obtained. This series is presented in Figure 11 with open circles. As it is seen in this figure, $\Delta\epsilon$ and b follow a linear increasing tendency with temperature, while $Log_{10}[\tau_\beta/s]$ linearly increases with the reciprocal absolute temperature. These dependences can be described by eqs 10−12.

$$\Delta\epsilon_\beta = 0.47 + 1.49 \times 10^{-3}T \tag{10}$$

$$b_\beta = 0.33 - 1.77 \times 10^{-4}T \tag{11}$$

$$\log_{10}[\tau_\beta/s] = -15.90 + \frac{2842}{273 + T} \tag{12}$$

To obtain a reliable set of parameters corresponding to the β*-relaxation, the influence of the β-relaxation is taken into account. The experimental values of ϵ'' in this region were fitted to the equation

$$\epsilon'' = \epsilon''_{\beta*} + \epsilon''_\beta \tag{13}$$

The extrapolated parameters from eqs 10−12 in the region of the β*-relaxation are allowed to vary less than 1%. Figure 10 shows the experimental data corresponding to the β*-relaxation at T = 75 °C. The fit of eq 13 to the experimental data, considering the influence of the extrapolated β-relaxation, is included as a continuous line. The separated contribution from the fitted β* and extrapolated β are represented as a dashed line and a

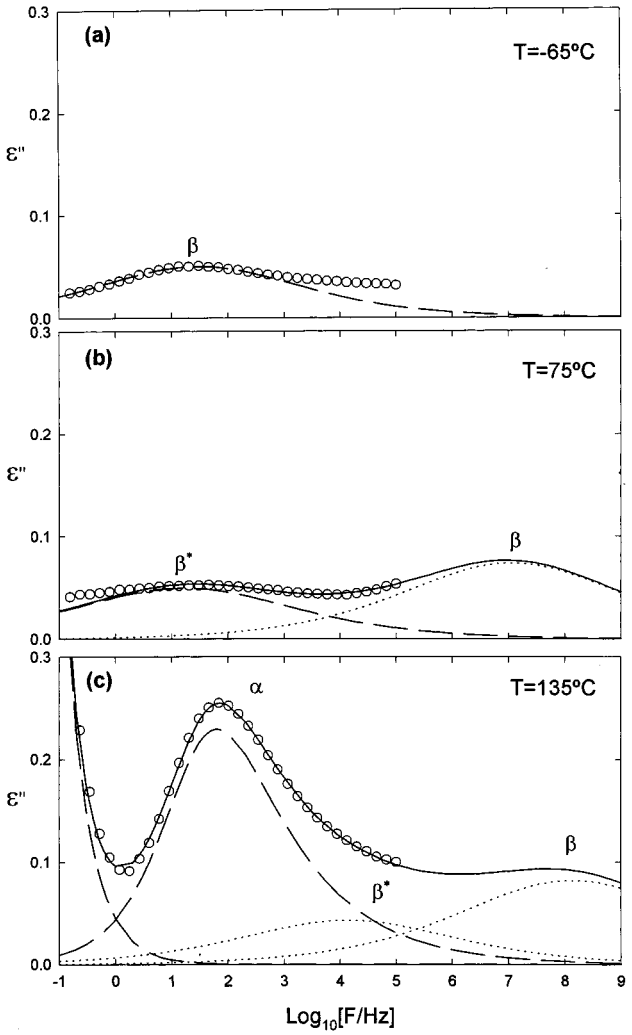

Figure 10. Experimental ϵ'' values of an amorphous sample, for the β-, β*-, and α-relaxations (○). Dashed lines correspond to fitted relaxations, dotted lines correspond to extrapolated relaxation, and continuous lines correspond to the total theoretical relaxation.

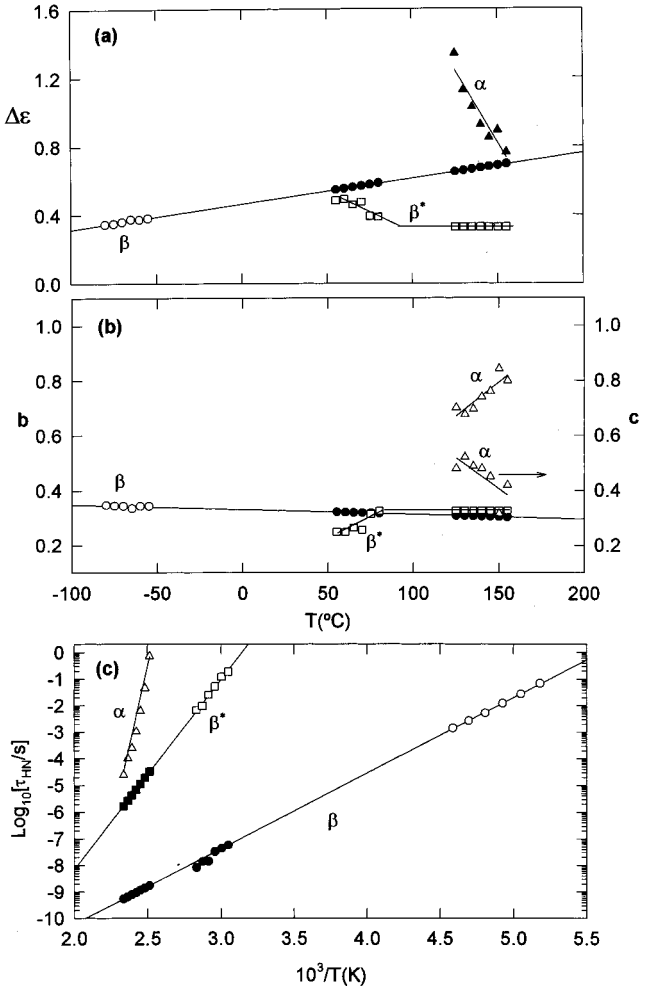

Figure 11. HN parameters obtained from the procedure explained in the Appendix. Open symbols correspond to fitting parameters whereas filled symbols correspond to extrapolated parameters: (○) β-relaxation; (□) β*-relaxation; (△) α-relaxation.

dotted line, respectively. Using this method for all the temperatures where the β*-relaxation presents a defined maximum in the experimental frequency window, a set of HN parameters for the β*-relaxation is obtained. These parameters are represented in Figure 11 with open squares. The extrapolated HN parameters for the β relaxation in this temperature region are also represented with solid circles. To obtain the parameters of the α-relaxation a similar procedure was followed. In this case

$$\epsilon'' = \epsilon''_{\alpha} + \epsilon''_{\beta^*} + \epsilon''_{\beta} \qquad (14)$$

Our intent was to follow a similar procedure for extrapolating the HN β* parameters to the temperature region where the α-relaxation is in our experimental frequency window. However, as can be seen in Figure 11, $\Delta\epsilon_{\beta^*}$ strongly decreases with temperature. The extrapolation of this behavior toward the region where the α-relaxation would lead to an $\Delta\epsilon_{\beta^*}$ value equal to 0. However, in Figure 10 it is clearly seen that there is still a strong contribution of the β*-relaxation on the temperature region where the α-relaxation is on the experimental frequency window. The same happens to the *b* parameter. Hence, the procedure in this case was the following.

The extrapolated parameters from the β relaxation and the value of τ_{β^*} were allowed to vary by 1%. On the other hand, the values of $\Delta\epsilon_{\beta^*}$ and b_{β^*} were considered as fitting parameters. The obtained parameters from the fitting of the experimental data to eq 14 are presented in Figure 11 as open symbols. The extrapolated values are also presented in Figure 11 as filled symbols. Figure 10 shows, for $T = 135$ °C, the resulting curve from the fitting using this procedure. The contribution of the a relaxation is included as a dashed line, and the contribution of both, β- and β*- relaxation are also included as dotted lines. The above-mentioned approach must be understood as an approximation and addresses the necessity for high frequency measurements to fully describe relaxation processes.

References and Notes

(1) Coburn, J. C.; Boyd, R. H. *Macromolecules* **1986**, *19*, 2238.
(2) Williams, G. *Adv. Polym. Sci.* **1979**, *33*, 59.
(3) Havens, J. R.; VanderHart, D. L. *Macromolecules* **1985**, *18*, 1663.
(4) Schlosser, E.; Schönhals, A. *Colloid Polym. Sci.* **1989**, *267*, 963.
(5) Ezquerra, T. A.; Majszczyk, J.; Baltá-Calleja, F. J.; López-Cabarcos, E.; Gardner, K. H.; Hsiao, B. S. *Phys. Rev. B* **1994**, *50*, 6023.
(6) Nogales, A.; Ezquerra, T. A.; García, J. M.; Baltá-Calleja, F. J. *J. Polym. Sci., Part B: Polym. Phys.* **1999**, *37*, 37.

(7) Suzuki, H.; Grebowicz, J.; Wunderlich, B. *Makromol. Chem.* **1985**, *186*, 1119.
(8) Lovinger, A. J.; Hudson, S. D.; Davis, D. D. *Macromolecules* **1992**, *25*, 1572.
(9) Hsiao, B. S.; Sauer, B. B.; Verma, R. K.; Zachamnn, H. G.; Seifert, S.; Chu, B.; Harney, P. *Macromolecules* **1995**, *28*, 6931.
(10) Marand, H.; Alizadeh, A.; Farmer, R.; Desai, R.; Velikov, V. *Macromolecules* **2000**, *33*, 3392.
(11) Strobl, G. R.; Schneider, M. J. *Polym. Sci., Polym. Phys. Ed.* **1980**, *18*, 1343.
(12) Santa Cruz, C.; Stribeck, N.; Zachmann, H. G.; Baltá-Calleja, F. J. *Macromolecules* **1991**, *24*, 5980.
(13) Cheng, S. Z. D.; Cao, M. Y.; Wunderlich, B. *Macromolecules* **1986**, *19*, 1868.
(14) Tzou, D. L.; Seai, P.; Abhiraman, A. S.; Huang, T. H. *J. Polym. Sci., Polym. Phys. Ed.* **1991**, *29*, 49.
(15) Sherman, L. M. *Plastics Technol.* **1995**, *May*.
(16) Santa Cruz, C.; Baltá-Calleja, F. J.; Zachmann, H. G.; Chen, D. *J. Mater. Sci.* **1992**, *27*, 2161.
(17) Buchner, S.; Wiswe, D.; Zachmann, H. G. *Polymer* **1989**, *30*, 480.
(18) Chen, D.; Zachmann, H. G. *Polymer* **1991**, *32*, 1612.
(19) Dörlitz, H.; Zachmann, H. G. *J. Macromol. Sci.—Phys.* **1997**, *B36*, 205.
(20) Ezquerra, T. A.; Baltá-Calleja, F. J.; Zachmann, H. G. *Acta Polym.* **1993**, *44*, 18.
(21) Cañadas, J. C.; Diego, J. A.; Mudarra, M.; Belana, J.; Díaz-Calleja, R.; Sanchís, M. J.; Jaimés, C. *Polymer* **2000**, *41*, 2899.
(22) Denchev, Z.; Nogales, A.; Ezquerra, T. A.; Baltá-Calleja, F. J. *J. Polym. Sci., Part B: Polym. Phys.* **2000**, *38*, 1167.
(23) Havriliak, S.; Negami, S. *Polymer* **1967**, *8*, 161.
(24) Kirst, K. U.; Kremer, F.; Litvinov, V. M. *Macromolecules* **1993**, *26*, 975.
(25) Vallerien, S. U.; Kremer, F.; Boeffel, C. *Liq. Cryst.* **1989**, *4*, 79.
(26) Dobbertin, J.; Hensel, A.; Shick, C. J. *Thermal Anal.* **1996**, *47*, 1027.
(27) Laughlin, W. T.; Uhlmann, D. R. *J. Phys. Chem.* **1972**, *76*, 2317.
(28) Böehmer, R.; Ngai, K. L.; Angell, C. A.; Plazek, D. J. *J. Chem. Phys.* **1993**, *99*, 4201.
(29) Ngai, K. L.; Roland, C. M. *Macromolecules* **1993**, *26*, 2688.
(30) Nogales, A.; Ezquerra, T. A.; Batallán, F.; Frick, B.; López-Cabarcos, E.; Baltá-Calleja, F. J. *Macromolecules* **1999**, *32*, 2301.
(31) Schönhals, A.; Schlosser, E.; *Colloid Polym. Sci.* **1989**, *267*, 125.
(32) Schönhals, A.; Kremer, F.; Schlosser, E. *Phys. Rev. Lett.* **1991**, *67*, 999.
(33) Huo, P.; Cebe, P. *Macromolecules* **1992**, *25*, 902.
(34) Kalika, D. S.; Krishnaswamy, R. K. *Macromolecules* **1993**, *26*, 4252.
(35) Adams, G.; Gibbs, J. H. *J. Chem. Phys.* **1965**, *43*, 139.
(36) Schick, C.; Donth, E. *Phys. Scr.* **1991**, *43*, 423.
(37) Wing, J.; Mijovic, J. *Macromolecules* **2000**, *33*, 933.

MA001066H